Defence Science Journal, Vol. 60, No. 3, May 2010, pp. 330-336
© 2010, DESIDOC

Development of Cube Recrystallisation Texture and Microstructure of an Aluminium Alloy Suitable for Cartridge Case Manufacturing

Prantik Mukhopadhyay* and Arun Kumar Verma

Defence Institute of Advanced Technology, Pune-411 025
**E-mail: prantikmukherje@yahoo.com*

ABSTRACT

Electron backscattered diffraction investigations on just fully recrystallised orientation image microstructures, showed that the cube-oriented grains had the largest size in all microstructures of an aluminium alloy, which have potential use in the cartridge case manufacturing for defence purpose. The simulation of cube microstructure and texture of that aluminium alloy was tried. The recrystallisation texture and microstructure simulation by the 3-D cellular automaton model with the consideration of highest mobility of 40º<111> grain-boundary, predicted the volume fraction of the cube texture orientation which was validated by experiment.

Keywords: Recrystallisation, cube-orientation, cellular automaton

1. INTRODUCTION

Nowadays, aluminium alloys have found application in manufacturing cartridge cases. The annealing and metal forming processes like cold drawing are done for the manufacture of aluminium alloy cartridge cases. The intermediate annealing process increases the ductility, which is needed for the final drawing of the cartridge cases. The recrystallisation occurs during the annealing process of aluminium alloy. The recrystallisation process changes the microstructure and texture of the aluminium alloy. The variation in the microstructure and texture due to recrystallisation can affect the forming properties during the cold drawing of the cartridge cases. Hence, the formation of recrystallisation texture and microstructure of the aluminium alloy cartridge cases are the subjects of research by experiment and simulation.

The recrystallisation texture of aluminium generally produces its characteristic cube texture, {001} <100> orientation. The understanding of the cube-orientation formation during recrystallisation of aluminium alloy is necessary to eliminate forming-related problem such as earing. The origin of recrystallisation texture of aluminium has been investigated extensively[1-10]. The theories behind the formation of the recrystallisation texture and microstructure of fcc metals, are briefly described here.

The oriented nucleation theory is based on the observation that certain orientations of transition band form recrystallisation nuclei[11, 12]. The availability of this transition band in deformed microstructure of fcc metals has been reported in literature[13-15]. Other investigations report that grain does not rotate as a whole but parts of a grain rotate in different directions and can produce deformation bands[16-20].

The theory of oriented growth considers that some grain-boundaries move faster than others and orientations associated with these grain-boundaries become prominent after recrystallisation[21-23]. Fastest growth of 40º<111> grain boundary between the existing cube after deformation and rolling texture orientations is important to determine the cube recrystallisation texture and microstructure of fcc metals.

The present study deals with the simulation of the cube-texture orientation and microstructure during recrystallisation of an aluminium alloy with the help of orientation-dependent grain boundary mobility, which has not been reported earlier. The simulation of experimentally observed cube texture and microstructure have been done by an advanced cellular automaton (CA) model to validate the oriented growth theory.

The advanced model, which has been used for microstructure and texture simulation, acts on the principle of CA method[24-26]. An advanced CA technique for the simulation of microstructure, texture, and kinetics has been developed by Mukhopadhyay[30], *et al.* That simulation tool can be efficiently applicable for the simulation of microstructure, texture, and kinetics of aluminium alloys for their industrial annealing process[27-30]. In principle, there are the two ways to define the minimum or the highest displacement by one-cell element. Marx[26], *et al.* decided to take the minimum displacement to be one cell element, which implies that higher grain boundary velocities would sweep several grid elements during each time step, while Mukhopadhyay[30], *et al.* considered the highest displacement to be one-cell element. This gave a microstructure development following the time-dependent discrete grain boundary mobility and driving pressure. The advantage of this technique is that it brings the fine grain morphology in microstructure simulation.

Received 6 March 2009, Revised 9 September 2009

2. EXPERIMENTAL METHOD

2.1 X-ray Texture Measurement

An aluminium alloy billet was processed by hot rolling in laboratory scale with the normal and cross rolling techniques. The composition of the aluminium alloy billet was *Zn* (5.5 %), *Mg* (2.2 %), *Cu* (1.6 %), *Cr* (0.23 %) and rest aluminium. The composition is in Wt %. A hot-rolled 2.5 mm thick strip was cut from the hot-rolled sheet and was cold-rolled to 40 per cent, 65 per cent and 80 per cent thickness reduction. The cold rolled texture pole figures were measured. Orientation distribution functions were derived by Bunge's series expansion method. Recrystallisation was performed in a furnace at 400 °C for 15 min for all cold-rolled sheets. The through thickness recrystallisation texture pole figures were measured and the orientation distribution functions were determined. The volume fraction of texture orientations like cube {001}<100>, brass (*Bs*) {011}<211>, *S* {123}<634>, goss {011}<100> and copper (*Cu*) {112}<111>, were derived for quantitative analysis.

2.2 Orientation Image Microscopy

A field emission gun scanning electron microscope equipped with electron backscattered diffraction (EBSD) feature was used for the measurement of the orientation image microstructure of all recrystallised specimens. The specimen surface requirement for the EBSD mapping was done by electropolishing at sub-zero temperature with 4:1 ethanol-perchloric acid electrolyte. The step size for EBSD mapping was kept at 1.0-1.2 μm[31].

3. RECRYSTALLISATION MICROSTRUCTURE MODELLING

An advanced model was used for the simulation of recrystallisation texture and microstructure[30]. The growth of the grain during recrystallisation was governed both by the mobility of the grain boundary and driving force. The velocity (v) of the recrystallisation front was given by[30]

$$v = j.K \tag{1}$$

where, j is the orientation-dependent grain-boundary mobility and K is the driving force. The mobility was defined as

$$j = \gamma\, j_o \exp\left(-\frac{Q_j}{kT}\right) \tag{2}$$

where, j_0 is the intrinsic mobility, k is the Boltzman constant, T is the temperature, Q_j is the activation energy, and γ is the orientation-dependent mobility factor.

The mobility data for intrinsic mobility and activation energy obtained from experiments were used for modelling[32]. The 40º<111> grain-boundary was considered to be associated with the highest mobility with angular deviation given by the Brandon criterion[33]. The 40º denoted the misorientation angle and the <111> was the axis of rotation. The low-angle grain-boundaries were taken as boundaries with minimum mobility. The average mobility was taken as a function of the highest mobility. The degree of oriented growth was determined as a mobility ratio of the average mobility to the highest mobility of grain-boundary. The degree of oriented growth was improved with the decrease in mobility ratio.

The discrete cold rolling texture orientations were taken as initial variables for recrystallisation simulation. The distribution of recrystallisation nuclei along the grain-boundaries of texture orientations was done according to the volume fractions of the deformation texture orientations. The site saturation of nucleation was considered for simulation. The total amount of slip of each deformation texture orientation, determined by the deformation texture model (GIA), was converted to dislocation density by the flow stress model (3IVM)[34-37]. An average of the orientation-dependent dislocation densities was considered as a cell variable for the recrystallisation simulation. The average deformation energy of the deformation texture orientations was derived from the average dislocation density (ρ_{avg})[35,37].

$$K_{avg} = 0.5\mu b^2 \rho_{avg} \tag{3}$$

where, μ is the shear modulus and b is the Burgers vector. A strong degree of oriented growth of the 40º <111> grain-boundary was applied during simulation. The average mobility was kept at the level of 5 per cent of the highest mobility.

4. RESULTS

4.1 Experimental Results

The constant phi2 sections (0°, 45° and 65°) of orientation distribution function (ODF) represent the development of the deformation texture (Fig. 1). The decrease of the cube-orientation and the increase in the *Cu, Bs*, and *S* rolling texture orientations are generally found after cold rolling of the commercial aluminium alloys[36]. A dissimilar trend is found here after the cold rolling of the cross-hot rolled strip. The overall texture intensity was reduced with the degree of deformation instead of being sharpened. The initial hot rolled strip had strong intensities of cube, *Bs* and *S* texture and less *Cu* texture. The decrease in the cube and *Bs* texture orientation intensities and the increase in the *Cu* texture orientation intensity with deformation have been observed here. The overall texture intensity variation with cold rolling is given in Table 1. Figure 2 shows the cube recrystallisation textures after recrystallisation experiments at 400 °C for 15 min for all percentage of reduction.

Table 1 shows that the recrystallisation texture intensity variation follows the intensity variation of the deformation texture. The volume fractions of significant texture orientations developed after deformation and recrystallisation are shown in Table 2. The experimental deformation texture volume fractions vary in a similar fashion as these are observed in the orientation distribution functions of Fig. 1. The volume fraction of the cube and the *Bs* texture decreases with the cold rolling though the intensity variation of *Bs* texture is not significant.

The increase in the *Cu* texture volume fraction with the cold rolling indicates that the shear rotation to *Cu* orientation is preferred here than the shear rotation to the *Bs* orientation, which is generally found in the deformation

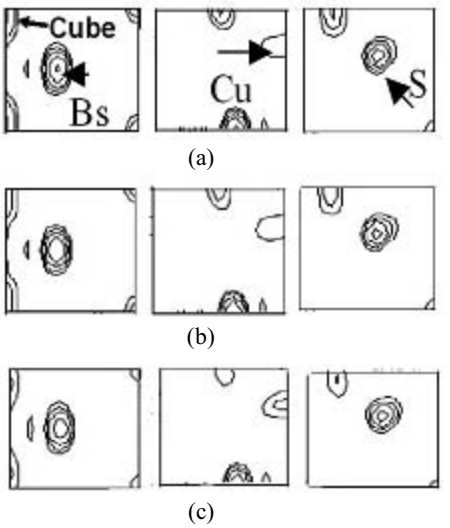

Figure 1. Shows 0º, 45° and 65º constant phi2 sections (of orientation distribution functions) of experimental cold-rolled texture: (a) 40 % cold-rolled (b) 65 % cold-rolled, and (c) 80 % cold-rolled.

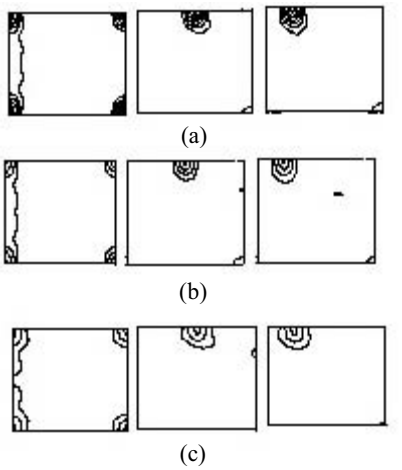

Figure 2. Shows 0º, 45° and 65º constant phi2 sections (of orientation distribution functions) of experimental recrystallisation texture (400 ºC, 15 min): (a) 40 % cold-rolled and recrystallised, (b) 65% cold-rolled and recrystallised, and (c) 80% cold-rolled and recrystallised.

Table 1. Highest intensity of orientation distribution functions after cold rolling and after recrystallisation (experiment and simulation)

Degree of deformation (%)	Cold-rolled	Recrystallisation	
		experiment	simulated
40	21.70	13.60	17.50
65	20.00	08.60	15.60
80	18.10	08.10	13.00

Table 2. Volume fractions of texture orientations

Orientations	40 % CRE	40 % RE	40 % RS	65 % CRE	65 % RE	65 % RS	80 % CRE	80 % RE	80 % RS
Cube	7.2	12.8	14.2	5.4	7.8	11	4.1	8.2	10
Goss	2.1	4	4.1	2.5	4.3	4.7	2.1	3.4	4.4
Cu	8.8	5.7	8	10	6.8	7.7	10.5	6.3	10.1
S	38.2	8.8	24.8	38	11	24.2	38.5	13.1	23.3
Bs	33.1	6.1	17.8	31	5.7	17	30	5.8	16.5

CRE: cold rolling experiments, RE: recrystallisation experiments, RS: recrystallisation simulation.
% denotes the deformation percentage of cold rolling before recrystallisation

texture of a commercial alloy. The strength of the goss and the *S* texture are not changed with the cold deformation. The experimental recrystallisation texture orientations of Table 2 show a sharp increase in the cube and goss texture orientations and a fall of cold deformation texture orientations (*Cu, S*, and *Bs*). The overall recrystallisation texture intensities (Table 1) and the volume fraction of the recrystallisation texture orientations cube and goss decrease with the increase in the degree of deformation prior to the recrystallisation. This trend is not rare to find and the causes are the randomisation of texture due to the presence of deformation zone surrounding the second-phase precipitates and the decrease of the

original cube texture with the cold rolling. The volume fractions of recrystallisation texture orientations cube and goss texture are well predicted in the recrystallisation simulation but strength of *Bs* and *S* orientations are not well reproduced in simulation (Table 2). The large variation between experimental and simulated recrsytallisation texture of *Bs* and *S* can be attributed to the role of other special grain-boundaries along with the 40º <111> grain-boundary in recrystallisation of this alloy.

The orientation image microstructures after recrystallisation at 400 °C for 15 min and at 500 °C for 10 s, show that the formation of recrystallisation microstructures depends on the degree of deformation and the recrystallisation temperature (Fig. 3). The recrystallisation microstructure becomes stable after 60 % pre-recrystallisation deformation but it varies strongly with temperature. The cube-oriented grains (with maximum 15° orientation scatter) have been observed to have the largest grain size in the recrystallisation microstructures and those are marked by 'x' sign.

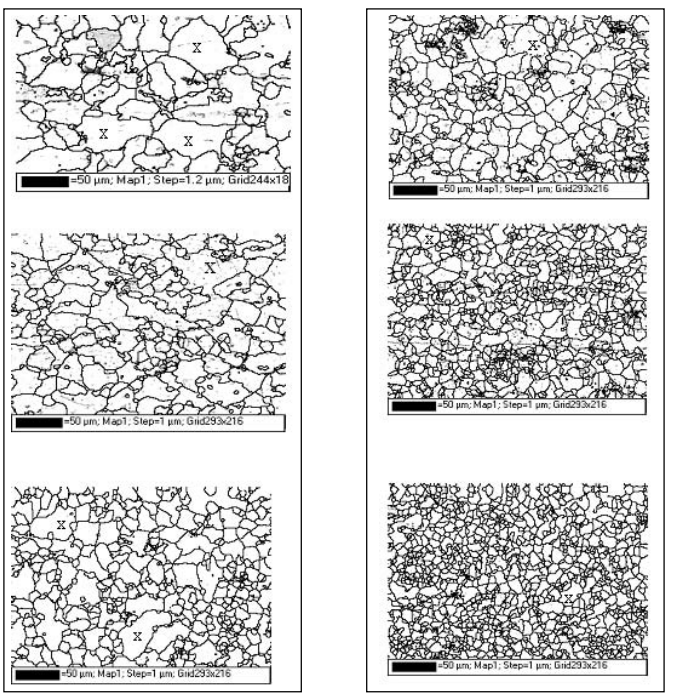

(a) (b)

Figure 3. Just recrystallised orientation image microstructure from experiment: (a) 400 °C, 15 min salt bath annealing for just recrystallisation (without significant grain growth) of 40 per cent, 65 per cent, and 80 per cent deformed samples, and (b) 500 °C, 10 s salt bath annealing for just recrystallisation (without significant grain growth) of 40 per cent, 65 per cent, and 80 per cent deformed samples. Cube- oriented (max 15° scatter from exact Cube-orientation) grains are marked by 'x'.

The determination of nuclei orientation distribution during the early stage of nucleation is shown in Fig. 4. No preference of orientation is observed from the nuclei orientation distribution. The orientation distribution of nuclei shows that the cube-orientation does not form nuclei first. The presence of the other phase does not form nuclei of any specific orientation. The measured nuclei orientations can also be used as the initial variable for the CA modelling. Since there was certain amount of growth occurred before the measurement of nuclei, to start the modelling from the beginning, the cold rolling texture orientations were chosen as the nuclei orientation.

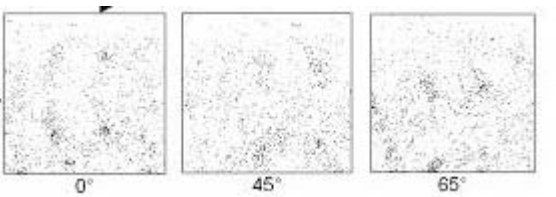

Figure 4. Orientations measurement from the early stage of recrystallisation (400 ºC). The 0°, 45°, and 65° constant phi2 sections (of orientation distribution function) of grain orientation obtained from EBSD experiments. No preference of the ideal orientations (Cube, *Cu*, *Bs,* and *S*) is observed during nucleation.

4.2 Modelling Results

Since the recrystallisation texture intensities vary according to those of the deformation texture, the recrystallisation simulation was done considering the cold-rolling texture orientations as initial orientations and distributing the recrystallisation nuclei of rolling texture orientations according to the volume fractions of cold-rolling texture orientations. The measured nuclei orientations can also be used as the initial variable for the CA simulation. Since there was certain amount of growth occurred before the measurement of nuclei, to start the simulation from the beginning, the cold rolling texture orientations were chosen as the nuclei orientation. The grain-boundary nucleation was used in simulation to get the effect of grain-boundary mobility. The strong oriented growth was applied. The resulting recrystallisation textures from simulation (Fig. 5) show stronger texture intensities than those obtained from recrystallisation experiments (Table 1). Table 2 shows the volume fraction of texture orientations after recrystallisation simulation. The strong oriented growth of 40º <111> grain-boundary affected the volume fraction of the cube and goss-orientations significantly. The volume fractions of the cube-and goss-orientations from simulation were similar to the experimental volume fractions of the cube- and goss-orientations. The reduction in the other rolling texture intensities in both the recrystallisation modelling and experiments strengthens the confidence of the simulation. The results of Table 2 show that the model is capable of predicting the cube- and goss-orientations quantitatively while it gives a qualitative decrease trend for other rolling texture orientations. The recrystallisation microstructures obtained from modelling are shown in Fig. 6. Both strong oriented growth as well as without oriented growth were used in the modelling. The 'x' sign highlighted a grain, which was affected by strong oriented growth.

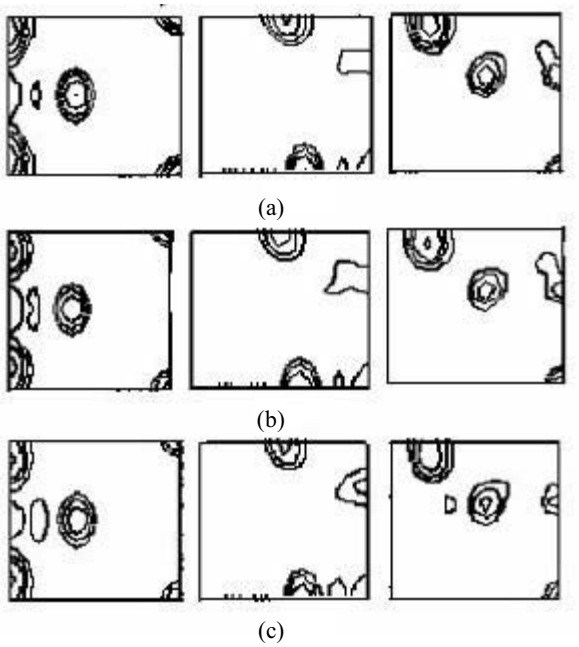

(a)

(b)

(c)

Figure 5. Shows 0°, 45° and 65° constant phi2 sections (of orientation distribution function) of recrystallisation texture (400 °C) from simulation: (a) 40 % cold-rolled and recrystallised, (b) 65 % cold-rolled and recrystallised, and (c) 80 % cold-rolled and recrystallised.

Investigation on the origin of recrystallisation microstructure shows (Fig. 4) that the nucleation is not restricted to the cube orientations. This observation confirms that the growth preference of the cube-orientation was the cause of the largest size of the cube grains in the recrystallisation microstructure.

The knowledge gained from the experiments regarding the oriented growth was used here for the recrystallisation texture and microstructure simulation. The strengths of the cube texture orientations obtained by simulation using strong oriented growth are greater than those from experiments (Tables 1 and 2), which show that the cube texture intensities or volume fractions are efficiently predicted by the advanced CA. Figure 6 presents two types of recrystallisation microstructures as results of modelling, one without the strong oriented growth (Fig. 6(a)) and the other with strong oriented growth (Fig. 6(b)). The 'x' sign in the microstructures (Fig. 6) shows a recrystallised grain with preferred oriented growth.

Since the input variables for simulation, like the initial deformed grain size, deformed orientations, deformation energy, nuclei orientations and locations are similar for both the cases, the only variable which brought the increment in grain size in Fig. 6(b), is the orientation dependent grain-boundary migration. The grains, which are close to the cube-orientation (15° scatter from the exact cube-orientation), were preferred by the oriented growth and those determine

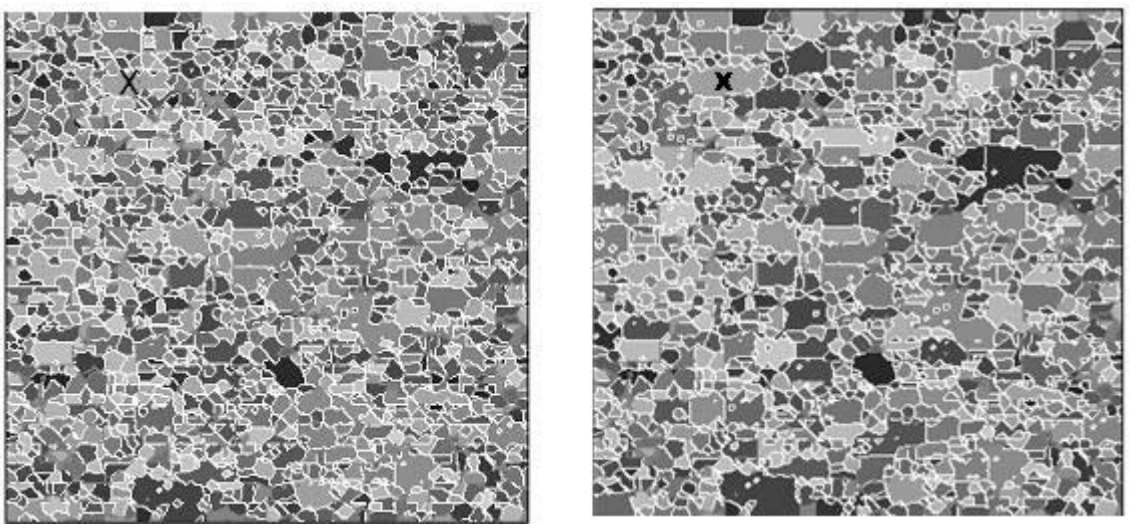

(a) (b)

Figure 6. Simulated recrystallisation microstructure with similar initial grain size and similar grain boundary nuclei orientation: (a) without strong oriented growth, and (b) with strong-oriented growth. Grain affected by oriented growth is indicated by 'x' sign. There are several near-cube-oriented grains. Preferential growth of near- or exact cube-oriented grains have occurred and have been shown in Fig. 6(b).

5. DISCUSSIONS

The presence of the cube-orientation as the largest grain in the microstructure of Fig. 3 brings the possibility that either the cube-orientation has growth preference during the microstructure formation or the cube grains nucleate first during the early stage of recrystallisation. the texture of this alloy after recrystallisation. This recrystallisation microstructure and texture simulation results strengthen the view that the retained cube-orientation of the deformed microstructure fulfills the 40°<111> grain-boundary condition with certain rolling texture orientations and the migration of this faster moving grain-boundary

between the existing cube and rolling texture orientation enhanced the cube-orientation to become prominent in the microstructure after recrystallisation.

The cold deep-drawing process in several steps with intermediate annealing are being used for cartridge case manufacturing. The presence of {001} <100> texture in this aluminium alloy can create the forming related problem such as earing. Hence a proper understanding of the formation of cube texture and grain-boundary engineering, which are the foci of the present research, are necessary to eliminate the earing problem.

6. SUMMARY

The experimental results showed that the overall texture intensity was reduced after the cold deformation.The recrystallisation texture intensities varied in a similar manner as the rolling texture intensity of this alloy.

The recrystallisation microstructures obtained from the experiment and simulation showed that the grains with the cube-orientation (15° max scatter from the exact cube-orientation) were the largest grains and the nucleation of recrystallisation was not preferential.

The site saturation of grain boundary nucleation was used in simulation of recrystallisation texture and microstructure. The nuclei were distributed along the grain boundaries of deformed grains according to the volume fractions of the rolling texture orientations, derived by experiment.

The development of recrystallisation texture orientations cube and goss were efficiently predicted by the advanced CA simulation with the help of orientation-dependent grain boundary mobility. The highest mobility was used for the 40º <111> grain-boundary and for the rest an average grain-boundary mobility of the order of 5 per cent of the highest mobility was applied.

Though the reduction in rolling texture intensities was observed, the intensities of rolling texture were not properly predicted by simulation. This could be attributed to the role of other special grain-boundaries along with the 40º <111> grain-boundary in recrystallisation of this alloy.

ACKNOWLEDGEMENT

The authors acknowledge the experimental and simulation facility of Institute fuer Metallkunde and Metallphysik, RWTH, Aachen University, Germany, and the research analysis facility of Defence Institute of Advanced Technology, Pune.

REFERENCES

1. Humphrey, F.J. & Hatherly, M. Recrystallisation and related annealing phenomena. Oxford, Elsevier, 2004.
2. Engler, O. & Huh, M.Y. *Mat. Sci. Eng. A,* 199, 271, 371.
3. de La Chapelle, S. *Scripta Materialia,* 2001, **45**, 1387.
4. Liu, W.C.; Man, C.-S.; Raabe, D. & Morris, J.G. *Scripta Materialia*, 2005, **53**, 1273.
5. Doherty, R.D.; Chen, L.C. & Samajdar, I. *Mat. Sci. Eng.* A, 1998, **257**, 18.
6. Maurice, C. & Driver, J.H. *Acta Materialia,* 1997, **45**, 4627.
7. Lucke, K. & Engler, O. *In* Proceedings of 3rd International Conference on Aluminium Alloys, Trondheim, 1992. pp. 439.
8. Vatne, H.E.; Shahani, R. & Nes, E. *Acta Materialia,* 1996, **44**, 4447.
9. Maurice, C. & Driver, J.H. *Acta Metall. Mater.,* 1993, **41**, 1653.
10. Arai, I.; Koizumi, M.M. & Inagaki, H. *In* Proceedings of 6th International Conference on Aluminium Alloys, edited by T. Sato; S. Kumai; T. Kobayashi & Y. Murakami. Toyohashi, 1998. 1269p.
11. Dillamore, L. & Katoh, H. *Metal Science,* 1974, **8**, 73.
12. Lee, C.S.; Smallman, R.S. & Duggan, B.J. *Scripta Materialia,* 1993, **29**, 43.
13. Inokuti, Y. & Doherty, R.D. *Acta Metallurgica,* 1978, **26**, 61.
14. Ridha, A.A. & Hutchinson, W.B. *Acta Metallurgica*, 1982, **30**, 1929.
15. Hjelen, J.; Orsund, R. & Nes, E. *Acta Metallurgica,* 1991, **39**, 1377.
16. Raabe, D.; Zhao, Z. & Mao, W. *Acta Materialia,* 2002, **50**, 4379.
17. Wert, J.A. *Acta Materialia,* 2002, **50**, 3125.
18. Standford, N.; Dunne, D. & Ferry, M. *Mater. Sc. Eng. A,* 2002, **1**.
19. Delannay, L.; Mishin, O.V.; Juul Jensen, D. & van Houtte, P. *Acta Materialia,* 2001, **49**, 2441.
20. Huges, D. *Acta Metall. Mater.,* 1993, **41**,1421.
21. Ibe, G. & Lucke, K. *In* Recrystallisation, Grain Growth and Textures, edited by H. Margolin. ASM, Metal Park, 1966. pp. 434.
22. Lucke, K. *In* Proceedings of ICOTOM-7, edited by Brakman *et al.*, Noordwijkerhout, 1984. pp. 195.
23. Sebald, R. & Gottstein, *G. Acta Materialia*, 2002, **50**, 1587.
24. Hesselbarth, H.W. & Gobel, I.R. *Acta Metall. Mater.,* 1991, **39**, 2135.
25. Raabe, D. *Phil. Mag. A*, 1999, **79**, 2339.
26. Marx, V.; Reher, F.R. & Gottstein, G. *Acta Materialia,* 1999, **47**, 1219.
27. Mukhopadhyay, P.; Loeck, M. & Gottstein, G. *J. Physique IV,* 2004, **120**, 225.
28. Mukhopadhyay, P. & Samajdar, I. *Metal Transactions,* 2008, **61**, 329.
29. Mukhopadhyay, P. *Aluminium,* 2006, **82**, 10.
30. Mukhopadhyay, P.; Leock, M. & Gottstein, G. *Acta Materialia,* 2007, **55**, 551.
31. Operating Manuel, Channel 5, HKL Technology, 2001.
32. Gottstein,G. & Shvindlerman, L. Grain boundary migration in metals, thermodynamics, kinetics, applications. Boca Raton (FL), CRC, 1999, 198 p.
33. Brandon, D.G. *Acta Metallurgica,* 1966, **14**, 1479.
34. Crumbach, M.; Mukhopadhyay, P.; Aretz, H.; Pomana,G.; Wagner, P. & Gottstein, G. *In* Proceedngs of 1st International Conference on Recrystallisation and Grain Growth,

edited by G. Gottstein & D. Molodov. Springer Verlag, Berlin, 2001, pp. 1061.
35. Goerdeler, M. & Gottstein, G. *In* Proceedngs of 1st International Conference on Recrystallisation and Grain Growth, *edited by* G. Gottstein & D. Molodov. Springer-Verlag, Berlin, 2001. pp. 1053.
36. Mukhopadhyay, P. *Aluminium,* 2002, **78**(10), 912.
37. Mukhopadhyay, P. IMM, RWTH, Aachen, Germany, 2005. (Doctoral Dissertation).

Contributors

Dr Ing Prantik Mukhopadhyay is currently working as Scientist D in Department of Materials Science, Defence Institute of Advanced Technology, Girinagar, Pune.

Mr Arun Kumar Verma is currently working as STA 'B'in the Department of Materials Science, Defence Institute of Advanced Technology, Girinagar, Pune.